



Oxygen-containing Functional Groups Enhancing Electrochemical Performance of Porous Reduced Graphene Oxide Cathode in Lithium Ion Batteries



Dongbin Xiong^a, Xifei Li^{a,b,*}, Hui Shan^a, Yang Zhao^a, Lei Dong^a, Hui Xu^c, Xianfa Zhang^c, Dejun Li^{a,**}, Xueliang Sun^{d,a}

^a Energy & Materials Engineering Centre, College of Physics and Materials Science, Tianjin Normal University, Tianjin 300387, China

^b Key Laboratory of Advanced Energy Materials Chemistry (Ministry of Education), Collaborative Innovation Center of Chemical Science and Engineering, College of Chemistry, Nankai University, Tianjin 300071, China

^c Key Laboratory of Functional Inorganic Material Chemistry, Ministry of Education & School of Chemistry and Material Science, Heilongjiang University, Harbin 150080, China

^d Nanomaterials and Energy Lab, Department of Mechanical and Materials Engineering, Western University, London, Ontario, N6A 5B9, Canada

ARTICLE INFO

Article history:

Received 15 May 2015

Received in revised form 30 May 2015

Accepted 10 June 2015

Available online 16 June 2015

Keywords:

Thermal Exfoliation

Graphene

Oxygen-containing Functional Groups

Lithium Ion Batteries

Cathode Materials

ABSTRACT

Exploring high performance and environment-friendly electrode materials is highly desirable for the sustainable Li-ion batteries (LIBs) system. In this study, a facile approach of the modified Hummers' method combining with special thermal reduction was proposed to synthesize nanostructured reduced graphene oxide (RGO) with abundant oxygen-containing functional groups. The resultant RGO showed high specific capacity and excellent cyclability as cathode materials for LIBs. The specific capacity of about 220 mAh g⁻¹ at a current density of 50 mA g⁻¹ was achieved after 100 cycles. More importantly, it was demonstrated that the capacity increased with the increase of the amount of oxygen functional groups, highlighting the significant effects of oxygen-containing functional groups of RGO on high lithium storage performance.

© 2015 Elsevier Ltd. All rights reserved.

1. Introduction

With the decrease of the use of fossil fuels as well as the increasing demand for clean energy in the twenty-first century, Lithium ion batteries (LIBs), due to their characteristics of high-energy density, high working potentials, and long cycle life, etc [1,2], have been proved to be one of the most advanced battery technology [3]. The current LIB technology highly depends on the use of lithium transition metal oxides or phosphates (e.g., LiCoO₂, LiNi_xMn_yCo_{1-x-y}O₂ or LiFePO₄) as cathodes with the high redox potentials [4], but these cathode materials show very limited energy capacities. Further, these are not environmentally benign, and the mineral resources of Co and Ni are scarce, resulting in high cost LIBs with limited performance. Therefore, the search for new energetic electrode materials, especially cathode materials, for LIBs has been highlighted in battery chemistry [5].

Two dimensional (2D) graphene materials have been one of the most promising miracle materials originating from its unique single-atom-thick sheet of carbon atoms arrayed in a honeycomb pattern [6,7]. Benefiting from remarkable advantages of large specific surface area (2630 m² g⁻¹), excellent electrical conductivity (10⁶ S cm⁻¹), high charge mobility (200000 cm² V⁻¹ s⁻¹), good chemical and environmental stability [6–8], graphene materials have been demonstrated to be a new class of outstanding candidate for electrochemical power source fields. As a result, they have been widely explored for applications in energy-related areas, including solar cells [9,10], LIBs [11–13], supercapacitors [14,15], etc. More importantly, graphene materials have shown great promises to improve the performance of the aforementioned energy systems, which satisfies the urgent demand for renewable energy production and efficient energy storage in modern society [14]. It is well known that graphene materials has been widely researched as LIB anodes [16–18], and show much higher reversible capacity than the commercial graphite, as previously demonstrated by our group [17,19], and various graphene-based composite materials presented enhanced battery performance [20–23]. Recently, differing from the anode side, it was reported

* Corresponding author. Tel.: +86 22 23766526; fax: +86 22 23766503.

** Corresponding author.

E-mail addresses: xfli2011@hotmail.com (X. Li), dejunli@mail.tjnu.edu.cn (D. Li).

that reduced graphene oxide (RGO) with oxygen-containing functional surface groups can work as cathode materials of LIBs [24]. During charge/discharge processes, as the redox centers, the oxygen-containing functional surface groups (such as $>C-O$ and $-COOH$) of RGO can rapidly and reversibly capture lithium ions through surface adsorption and/or surface redox reaction. Thus, functionalized graphene exhibit higher energy density with long-lasting cyclability in comparison with the current cathode materials [25,26]. For example, Bor Z. Jang's group proposed a novel LIB using nanostructured graphene as both the anode and the cathode [25]. The obvious difference is that the cathode was functionalized graphene. They obtained an energy density of 160 Wh kg^{-1} and a power density of 100 kW kg^{-1} . In the recent reports, it was indicated that the functionalized graphene with more oxygen-containing groups can deliver high performance as LIB cathodes [24,27]. However, the aforementioned functionalized graphene cathodes with enhanced performance are only based on chemical reduction with tedious and low yield, which shows some difficulties in scale-up, and detailed reactive mechanisms have not been discussed.

In this report, we developed a facile approach of special thermal reduction to design partial reduced graphene oxide (RGO). It is worth noting that during the process of special thermal reduction, the controllable air gas was specially introduced to control oxygen-containing functional groups onto RGO. The as-prepared partial RGO as cathode materials for LIBs are expected to show a superior cycle stability and higher energy performance compared with previous reports [24,27]. It was demonstrated that oxygen-containing functional groups on RGO is the significant key as reaction center with lithium ions. More importantly, this approach shows some promising possibilities for mass production of the proposed cathode material.

2. Experimental

2.1. Materials

Natural graphite powder (purity $\geq 99.95\%$) was supplied by Aladdin Chemistry Co., Ltd. (Shanghai, China). Concentrated sulfuric acid (95%~98%), fuming nitric acid (65~68%), KMnO_4 (99%), NaNO_3 (99%) and H_2O_2 (30%) were used as received from Tianjin Guangfu Chemical Research Institute (China).

2.2. Synthesis of graphite oxide (GO)

Graphite oxide (GO) was initially fabricated by modified Hummers method, as previously reported by our group [19]. The natural graphite (1 g) and NaNO_3 (0.75 g) were uniformly mixed, then 34 mL of H_2SO_4 (98%) was added into the mixture and stirred for 2 h in an ice bath, meanwhile, KMnO_4 (4.5 g) was slowly added to the dispersion. After the mixture was stirred for 5 days at room temperature, 100 mL of H_2SO_4 (5%) was added to the mixture and stirred for another 2 h. Then 5 mL of H_2O_2 (35%) were slowly added to the solution until there was no gas bubbles produced. The resultant graphite oxide was then repeatedly washed with HNO_3 (10%) aqueous solution. The resulting GO was then thoroughly centrifugated with deionized (DI) water to obtain GO suspension. The GO suspension was finally dried at room temperature for 24 h to obtain GO.

2.3. Synthesis of reduced graphene oxide (RGO)

The as-prepared GO was ground into fine powder. After the tube furnace was heated up to 950°C at a rate of $10^\circ\text{C min}^{-1}$, the fine powder was quickly put into the center location, and was thermally

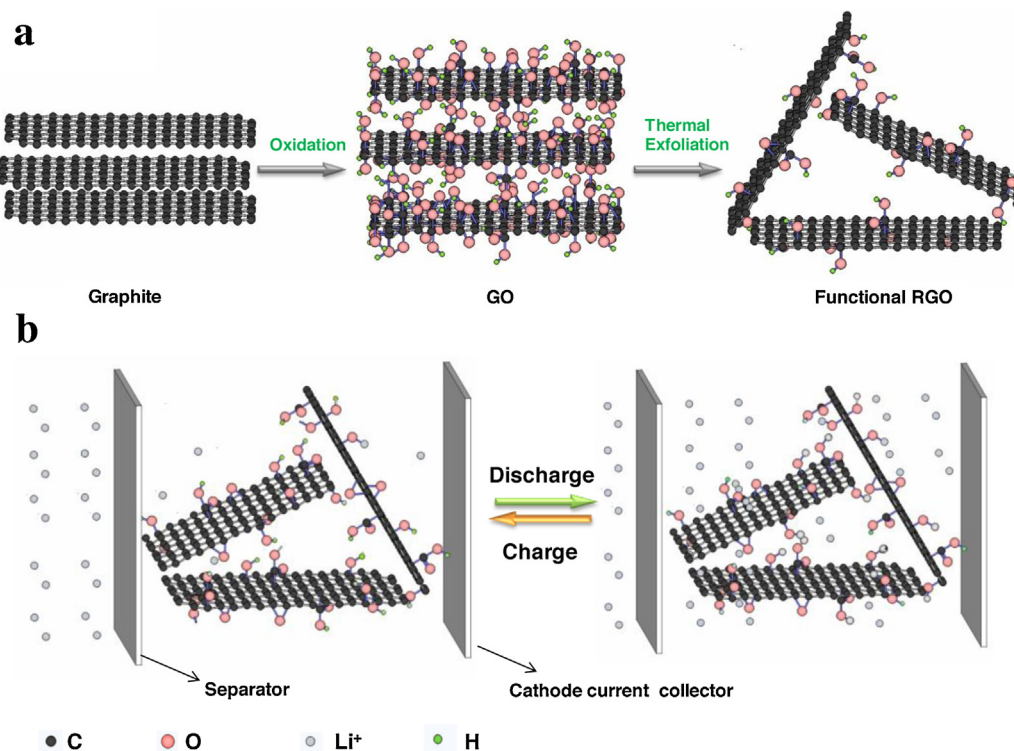


Fig. 1. (a) Schematic illustration of the oxidation mechanism and pore formation and reduction mechanism; (b) Schematic illustration for the lithium-storage mechanism of the reduced graphene oxide (RGO).

exfoliated for 1 minute under Argon atmosphere mixed with air (99%Ar+1%air) to obtain RGO. The RGO were further treated in gas mixture (95%Ar+5% H_2) at 900 °C for 2 h and 1000 °C for 8 h, respectively, to obtain the RGO with few functional groups, and the ramping rate was 10 °C min^{-1} . The RGO materials and the samples treated at 900 °C for 2 h and 1000 °C for 8 h were labeled as RGO-I, RGO-II, RGO-III, respectively.

2.4. Materials characterization

Scanning Electron Microscopy (SEM, SU8010, Hitachi Japan) and Transmission Electron Microscopy (TEM, JEOL JEM-3000F) were utilized to characterize the morphologies and structures of the samples. X-ray Diffraction (XRD) patterns were recorded on X-ray diffractometer (DX-2700) with Cu K α radiation. The functional groups were detected by Fourier transform infrared spectroscopy instrument (FTIR, IRAffinity-1, SHIMADZU). Raman spectra were recorded using LabRAM HR800. X-ray photoelectron spectroscopy (XPS, VG ESCALAB MK II) was performed to analyze O/C ratio of the samples. The hydrophilic testing was performed to characterize the effects of oxygenic functional groups of the samples by Attension Theta SFE (ksv INSTRUMENTS).

2.5. Electrochemical test

The cathode was prepared by mixing active material, carbon black, and polyvinylidene fluoride (PVDF) with a weight ratio of 80:10:10 using N-methylpyrrolidone (NMP) as solvent. A lithium foil was used as the counter electrode, and a solution of 1 M LiPF $_6$ in ethylene carbonate (EC)–diethyl carbonate (DEC) (1:1 in volume) was used as electrolyte. The electrode was dried at 100 °C for overnight under vacuum before a coin cell assembly in an argon-filled glovebox. The electrochemical performance of the samples was evaluated using CR2032 coin cells at a voltage range of 1.5 V~4.5 V (vs. Li/Li $^+$) with Land battery test system (LANHE CT2001A). Cyclic voltammogram (CV) measurements were performed on Princeton Applied Research VersaSTAT

4 electrochemical workstation using a voltage range of 1.5~4.5 V (vs. Li/Li $^+$) at a scan rate of 0.1 $mV s^{-1}$. Electrochemical impedance spectroscopy (EIS) measurements were performed on a Princeton Applied Research VersaSTAT 4 over a frequency range from 0.01 Hz to 100 kHz with the AC amplitude of 5.0 mV.

3. Results and Discussion

The schematic illustration in Fig. 1a shows the proposed synthesis mechanism of RGO-I by modified Hummers' method combining with a special thermal reduction process. During the oxidation process, the interlayer spacing of graphite carbon layer increased and a mass of oxygen-containing functional groups were introduced. In the following special reduction process, most of oxygen-containing functional groups were reduced. Interestingly, this process can still generate oxygen-containing functional groups onto RGO originating from the introduction of controllable air gas.

SEM and HRTEM were employed to characterize the structure and surface morphologies of various RGO. The SEM images of graphite oxide and graphene oxide are shown in Supporting Information Fig S1. During ultrasonic treatment, the stromatolitic graphite oxide (see Fig S1 a, b) was obviously stripped to graphene oxide in Fig S1 c and d. The SEM images in Fig. 2a and b show morphologies of the obtained RGO-II and RGO-I, respectively. Both images with low magnification show loose 3D porous appearance, and the increased magnification images indicate highly porous wrinkle structure and a crumpled paper-like external morphology. Fig. 2c and d illustrate the TEM images of obtained RGO-II and RGO-I, respectively. It can be clearly observed that both RGO-II and RGO-I exhibit a highly transparent gossamer sheets including only a few graphene layers, which is consistent with the graphene materials previously reported by our group [17,19]. Clearly, RGO-I exhibits a similar structural morphology to RGO-II and RGO-III shown in Fig S1 e and f, indicating that the further reduction process does not affect the 3D porous structure of RGO.

XRD patterns of the pristine graphite, GO, RGO-I, RGO-II, and RGO-III are depicted in Fig. 3a. The as-prepared GO exhibits a sharp

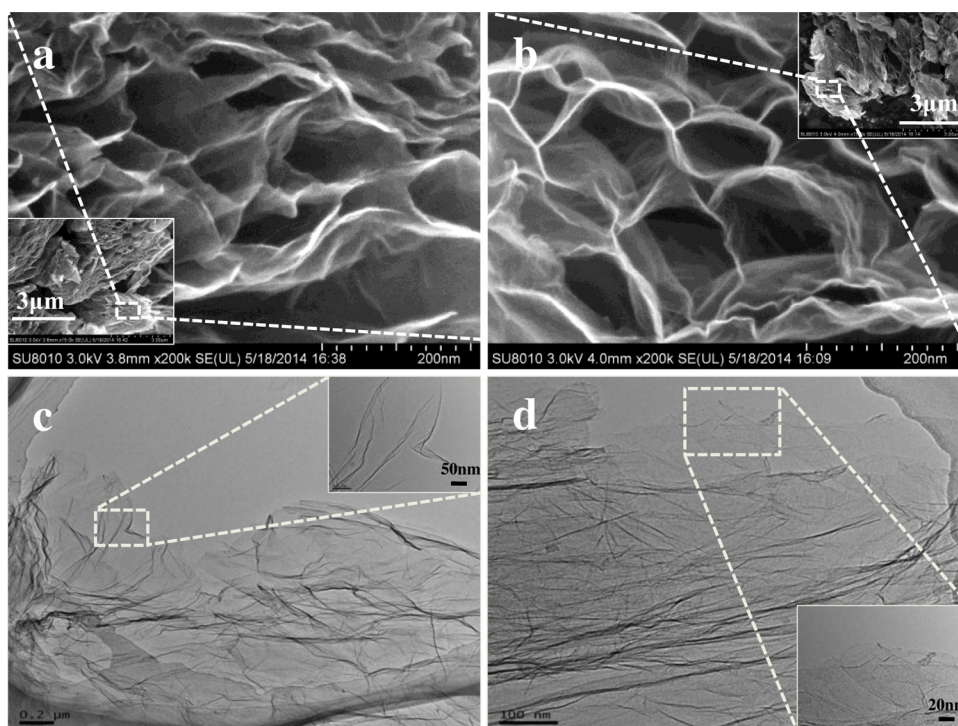


Fig. 2. SEM and TEM images of RGO-II (a, c) and RGO-I (b, d).

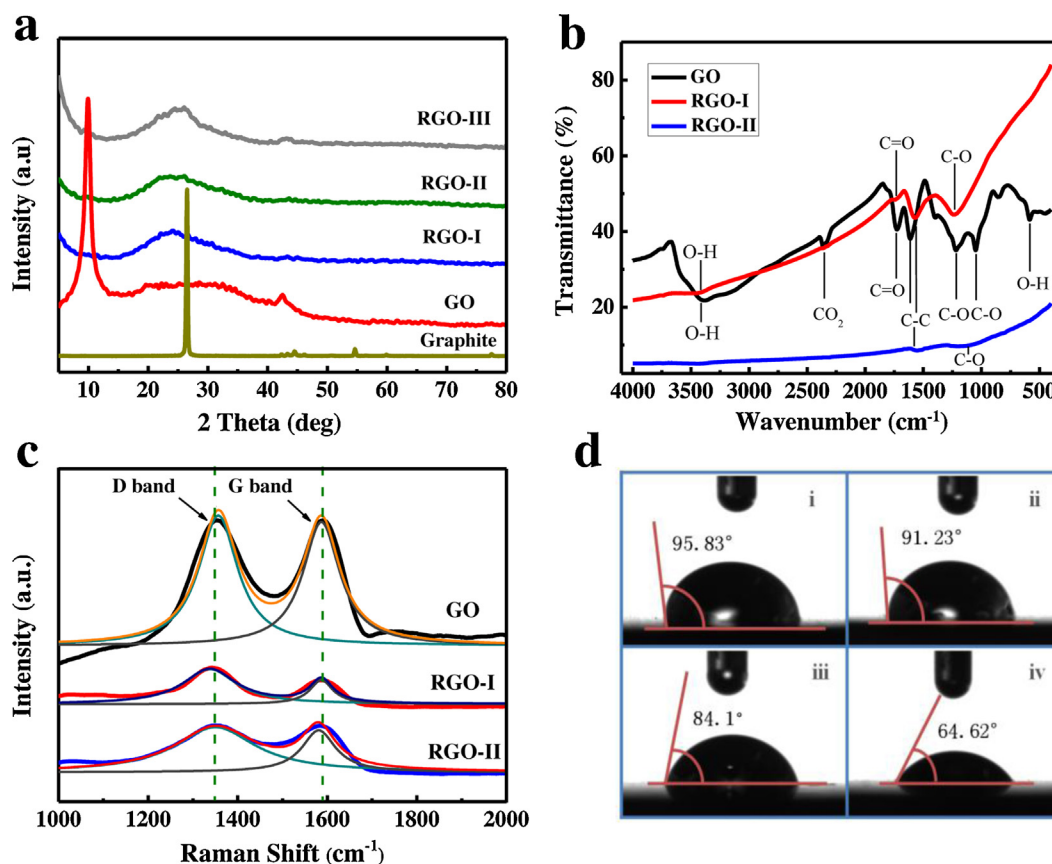


Fig. 3. (a) XRD patterns of pristine graphite, GO, RGO-I, RGO-II and RGO-III; (b) FT-IR spectra of GO, RGO-I and RGO-II; (c) Raman spectra of GO, RGO-I and RGO-II; (d) Pictures of contact angle of the samples: (i) RGO-III, (ii) RGO-II, (iii) RGO-I and (iv) GO.

reflection peak at 11.8° (corresponding to a d-spacing of 0.749 nm), which can be assigned to the (001) reflection of the solid GO. In comparison to the natural graphite, the decreased diffraction angle of GO (the diffraction peak of the natural graphite appears at 26.6°) results from the presence of the residual oxygen-containing functional groups [28,29], such as -OH, C=O, as well as the presence of interlayer water. The thermal exfoliation of GO greatly decreases the oxygen-containing functional groups and interlayer water. The XRD patterns of the RGO-I, RGO-II and RGO-III exhibit a peak centered at 23.6° , 24.4° and 25.2° , respectively, suggesting that the interlayer distance of the RGO gradually decreases because of the decrease of oxygen-containing functional groups [28,30], which will induce a weakened electrostatic repulsion between the graphene sheets.

The FT-IR spectra of GO, RGO-I and RGO-II are shown in Fig. 3b. The absorption bands at 1729 cm^{-1} are ascribed to the C=O stretching of -COOH and absorption bands $1399\text{--}1064\text{ cm}^{-1}$ are ascribed to the C-O stretching of the C-OH/C-O-C groups, respectively. The -OH stretching absorption of the C-OH groups appears at 3409 and 621 cm^{-1} . Compared to the GO, the RGO-I sample shows weaker C-O/C=O stretching absorption [31]. After further reduced by H_2 , the O-H absorption of the obtained RGO-II sample disappears, indicating that the functional groups on the surface of RGO can be reduced. It is worth noting that the RGO-II remains much less oxygen-containing functional groups than RGO-I [32].

Raman spectroscopy can provide some structural information of the graphene materials. Fig. 3c shows the Raman spectra of GO, RGO-I, and RGO-II. As shown in Fig. 3c, the typical features of three samples in Raman spectra show the G line around 1582 cm^{-1} and the D line around 1350 cm^{-1} . The G line is assigned to the E_{2g}

phonon of C sp^2 atoms, while the D line is a breathing mode of κ -point phonons of A_{1g} symmetry [33]. The relative intensity ratio of the D and G bands (I_D/I_G) reflects the defect density in the RGO [34], that is, the smaller the I_D/I_G ratio, the higher the degree of ordering in the carbon material. The I_D/I_G values of GO, RGO-I, RGO-II are 1.12, 3.36 and 2.57 respectively. The I_D/I_G value of the GO (1.12) was smaller compared with that of RGO-I(3.36) and RGO-II (2.57) due to a higher level of oxidation, which is in good agreement with the previous study focusing on the different degrees of oxidation of graphite oxid as reported by Karthikeyan Krishnamoorthy [33]. But, compared with RGO-I, I_D/I_G of RGO-II decreases, which indicates the higher degree of ordering, fewer defects and the presence of fewer oxygen-containing functional groups of RGO-II.

To characterize the oxygen-containing functional groups of the samples, the hydrophilic test was performed by dripping water on the surface of glass sheets which were coated with GO and various RGO samples. GO and RGO samples were coated to the same level to make the same surface roughness before dripping water, as shown in Fig. 3d i~iv. It is obvious that the hydrophilic angles of RGO-III, RGO-II, RGO-I and GO are 95.83° , 91.23° , 84.1° , 64.6° , respectively. It is well known that the smaller the hydrophilic angle, the better the hydrophilicity of the samples. Since an increase of oxygen-containing functional groups enhances the hydrophilicity of the samples, it can be concluded that the content order of oxygen-containing functional groups of the samples is $\text{GO} > \text{RGO-I} > \text{RGO-II} > \text{RGO-III}$. Among four samples, GO shows the most oxygen-containing functional groups, and RGO-III holds the least oxygen-containing functional groups. The oxygen content of graphene oxide, RGO-I and RGO-II was further unraveled by the element mapping images of carbon and oxygen (Supporting

Information, Figure S2), where one can see that oxygen-containing functional groups were uniformly distributed on the surface of RGO. As shown in Figure S3 of Supporting Information, energy-dispersive X-ray (EDX) analysis illustrates that the content order of oxygen-containing functional groups of the samples is GO > RGO-I > RGO-II > RGO-III.

The X-ray photoelectron spectroscopy (XPS) was performed to identify oxygen-containing functional groups of RGO. As shown in Fig. 4a, the survey spectra of RGO-I and RGO-II show the presence of O 1s peak. This peak was attributed largely to the presence of oxygen containing functional groups on the RGO nanosheets. The intensity of the O 1s peak becomes weaker from RGO-I to RGO-II, according with the results of quantitative elemental analysis in Table 1, the oxygen atomic percentage in the RGO-I and RGO-II is 7.01% and 4.11%, respectively, revealing that the reduced process results in more residual oxygen functional groups on RGO. To further gain insights into the structure of RGO, the O existence in both RGO-I and RGO-II can be demonstrated by the deconvolution of O 1s spectra shown in Fig. 4b and c. The O atoms occurred by the forms of O-C=O, C-OH and C=O can be clearly identified. Compared to the RGO-I in Fig. 4b, obviously, the peak intensities of the oxygen-containing functional groups greatly decreased in the spectra of RGO-II (Fig. 4c) after further reduction by H₂. RGO-II contained less content of O-C=O and C-OH than RGO-I; importantly, the C=O at 530.5 eV disappeared in O 1s spectra of RGO-II, as showed in Fig. 4b. It indicates that the special thermal exfoliation with the presence of a little air successfully generated RGO with abundant oxygen-containing functional groups.

The electrochemical performances of the as-prepared materials were evaluated by using galvanostatic charge-discharge measurements at a current density of 50 mA g⁻¹ over the voltage range 1.5–4.5 V (vs. Li/Li⁺). Using a larger voltage window allows for deeper understanding of the electrochemical reaction behavior between RGO cathode and lithium. Fig. 5a and b show the charge-discharge curves of the RGO-I and RGO-II electrodes in the 1st, 2nd, 10th, 20th, 50th and 100th cycles, respectively. Obviously, no clear potential plateau is observed in the charge/discharge processes of RGO-I and RGO-II cathodes, as previously reported [26], which results from the existence of electrochemically and geometrically nonequivalent lithium storage sites within the RGO [19]. The initial discharge capacity of the RGO-I is 163 mAh g⁻¹, and then gradually increase to 220 mAh g⁻¹, RGO-II with few oxygen-containing functional groups showed much lower electrochemical activity with initial discharge capacity of 49 mAh g⁻¹. As shown in Fig. 5c, RGO-I was examined by cyclic voltammetry at a sweep rate of 0.1 mV s⁻¹ within a voltage range from 1.5 to 4.5 V (vs. Li/Li⁺) to further understand the electrochemical lithium storage into the RGO cathode. It can be seen that RGO-I electrode shows a reversible lithiation/delithiation process, and the cyclic voltammetry (CV) curve obtained was similar to the reference [26] that no clear redox peak is observed. This is maybe due to the reason that carbonyl (C=O) groups were reversibly reduced and oxidized with

Table 1

XPS elemental analysis of RGO-I and RGO-II samples.

Samples	C1s [atom%]	O1s [atom%]
RGO-I	92.99	7.01
RGO-II	95.89	4.11

Li ions as previously reported [35,36]. More importantly, there is no obvious profile difference in the first three cycles, indicating that RGO-I electrode shows stable cycling performances.

Fig. 5d shows the cycling performance of GO, RGO-I, RGO-II and RGO-III samples at a current density of 50 mA g⁻¹ up to 100 cycles. It is observed that RGO-II and RGO-III exhibited much lower specific capacities less than 60 mAh g⁻¹. For the samples with rich oxygen-containing functional groups, GO and RGO-I samples showed superior performance compared to RGO-II and RGO-III, clearly demonstrating that the oxygen-containing functional groups on the surface of RGO cathodes function as lithium storage sites, which was in agreement with previous reports [27,37]. Moreover, in the initial several charge/discharge processes, the obtained capacities increased with cycles, which may be due to electrochemical activation process, namely the gradual penetration of electrolyte into the porous structure that promotes the activation of electrode materials, as well as Li⁺ conduction [17,38,39]. Especially for RGO-I sample, a significant increase of the specific capacity is observed from 169 mAh g⁻¹ to 220 mAh g⁻¹, and then the cathode remains constant capacity. As demonstrated in Fig. 3b, the GO surface possesses rich oxygen-containing functional groups. However, due to very low electrical conductivity, GO showed poor cycling performance and lower specific capacity in comparison to RGO-I; for instance, after 100 cycles the capacities of GO and RGO-I were 80 and 220 mAh g⁻¹, respectively. Obviously, among various cathodes studied [40,41], the RGO-I cathode in this study presents superior cycle performance for LIBs, which may be due to the factors that (i) the high specific surface area ensures good close contact between electrode and electrolyte. (ii) porous frameworks with good conductivity is beneficial for efficient electron and ion transport. (iii) considerable oxygen-containing functional groups increase reversible lithium storage.

Fig. 5e confirms the superior rate capability of RGO-I cathode with the discharge capacities of 220, 193, 147 and 118 mAh g⁻¹ at 50, 100, 200 and 400 mA g⁻¹, respectively. During charge/discharge processes, an increase of current density resulted in the decreased specific capacity, which is attributed to a low lithium ion diffusion rate [42]. Remarkably, when the current density is again reduced back to 50 mA g⁻¹ after 55 cycles, a stable and even higher capacity of 235 mAh g⁻¹ can be resumed. Fig. 5f displays the discharge capacities of the 10th cycle at various current densities and relative capacity retention compared with the capacity at 50 mA g⁻¹. The capacity retention of RGO-I were 87.7%, 66.8% and 53.6% at current densities of 100, 200, and 400 mA g⁻¹, respectively. Moreover, good

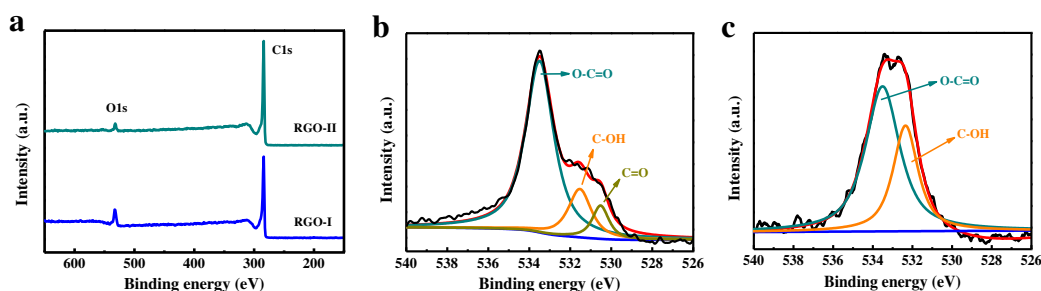


Fig. 4. (a) Survey scans of RGO-I and RGO-II; (b) The O1s XPS spectra of RGO-I; (c) The O1s XPS spectra of RGO-II.

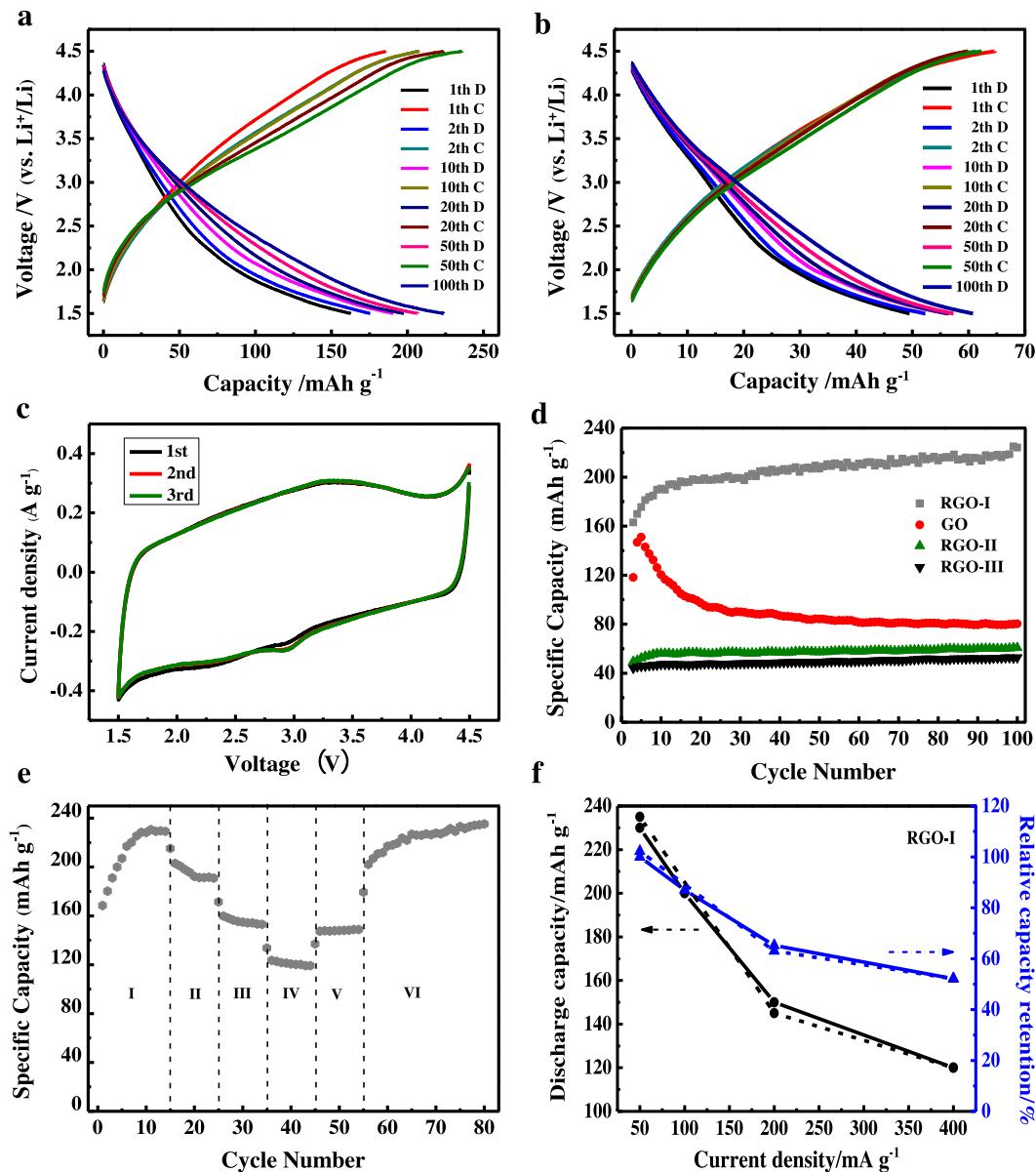


Fig. 5. Electrochemical performance of functionalized RGO (RGO-I, RGO-II and RGO-III) and GO: (a) voltage–capacity curves of RGO-I sample at 50 mA g^{-1} in different charge–charge cycles; (b) voltage–capacity curves of RGO-II sample at 50 mA g^{-1} in different charge–charge cycles; (c) CV data of the first 3 cycles for the RGO-I sample over a voltage range from 1.5 to 4.5 V with a scan rate of 0.1 mV s^{-1} ; (d) Cycling performance of GO, RGO-I, RGO-II and RGO-III electrodes at a current density of 50 mA g^{-1} ; (e) Rate capability of RGO-I electrode at different rates: (I) 50, (II) 100, (III) 200, (IV) 400, (V) 200, (VI) 50 mA g^{-1} ; (f) Discharge capacity and capacity retention of RGO-I at different current densities.

cyclability is still maintained when the current density is recovers to 50 mA g^{-1} . It can be concluded that RGO-I showed the good rate capability for the LIB cathodes.

To better understand the superior electrochemical performance of RGO-I, electrochemical impedance spectroscopy (EIS) of the GO, RGO-I and RGO-II electrodes were carried out after 10 charge/discharge cycles. As shown in Fig. 6, all Nyquist plots of the GO, RGO-I and RGO-II electrodes exhibit a broad depressed semicircle at the high frequencies for the charge-transfer kinetically controlled region and a straight line at the low frequencies for the mass-transfer-controlled Warburg region [43]. An equivalent circuit is present in inset of Fig. 6, where R_s is the electrolyte resistance of the electrochemical system, and R_{ct} is the charge-transfer resistance. The constant phase element (CPE_{ct}) normally indicates the double layer capacitor, and Z_w is the Warburg element [44]. After simulation using equivalent circuit, the R_{ct} of

GO, RGO-I and RGO-II is found to be 1833, 402.9 and 108Ω , respectively, which indicates that the electrical conductivity of RGO-I and RGO-II is improved considerably. Thus, a sharp difference of R_{ct} explains why GO shows poor performance, as we previously expected. RGO-II electrode exhibits a higher electrical conductivity and a lower R_{ct} , indicating the improved electrical conductivity due to further reduction of RGO-I. It was reported that the specific capacities of graphene cathode materials highly depends on two factors: surface oxygen-containing functional groups and electrical conductivity [24,27]. On one side, the GO material possesses abundant surface oxygen-containing functional groups, but low electrical conductivity. On the other side, the RGO-II showed higher electrical conductivity, but a limited amount of oxygen-containing functional groups. As a result, the GO and RGO-II cathode materials exhibit poor lithium storage performance for LIBs. It is reasonable that RGO-I showed

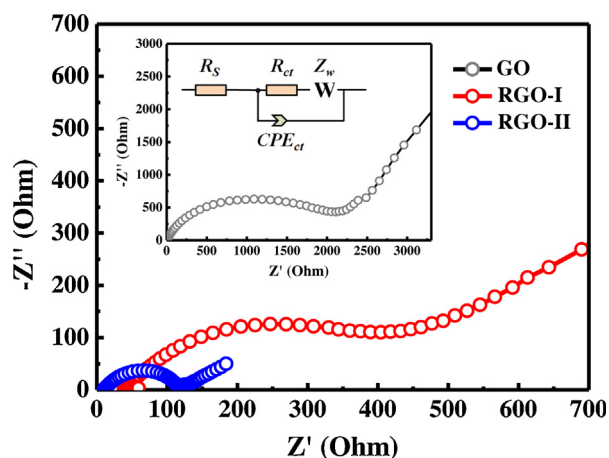


Fig. 6. Electrochemical impedance spectra (EIS) plots of the GO, RGO-I and RGO-II electrodes after 10 cycles at a full charge state (4.5 V); the inset shows the selected equivalent circuit to fit the EIS plots.

superior electrochemical performance due to the rich oxygen-containing functional groups on the surface and relatively high electrical conductivity.

In this report, the reduced graphene oxide (RGO) was created and controlled by combining modified Hummers' method with special thermal reduction via the controllable air gas. The excellent specific capacity of RGO-I is mainly attributed to the reaction between surface oxygen-containing functional groups and lithium ions as well as the three-dimensional pore structure of the reduced graphene oxide. As shown in the schematic illustration of Fig. 1, the three-dimensional pore structure acts as the channels for lithium ion transport and storage; more importantly, the surface functional groups like C=O and —OH can serve as the Faradaic reactions centers for efficient Li storage during charge/discharge processes. The XPS analysis showed that RGO-I contains a considerable amount of oxygen (the atomic ratio of C/O is around 13). Moreover, our study confirmed that for the RGO-II sample, some functional groups of RGO-I were removed with heat treatment in 95%Ar+5%H₂ without changing the morphology of RGO, as previously mentioned in Fig. 2. The capacity comparison of RGO-I and RGO-II demonstrates the significant role of oxygen-containing functional groups even RGO-II show much higher electrical conductivity in EIS study. During charge/discharge processes, these oxygen-containing groups can electrochemically react with lithium ions. It is obvious that increasing oxygen-containing groups results in an increase of the discharge capacity, and the oxygen-containing functional groups of RGO cathodes are the significant key for lithium storage functioning as reacting center.

4. Conclusions

In summary, we developed a novel strategy for the preparation of RGO cathode materials. The effectiveness of this strategy is to take full advantage of highly conducting and porous graphene framework with electrochemical active functional groups for reversible and fast Li storage through the oxygen functional groups of RGO. These RGO materials were demonstrated to exhibit excellent electrochemical performance in terms of high capacity, good rate capability and cycling stability. Importantly, this approach shows some possibilities for mass production of the proposed cathode material which is much more environmental and cost less than the conventional cathode materials. It is believed that the proposed simple and novel approach will be promising for rechargeable high energy density LIBs.

Acknowledgments

This research was supported by Key Projects of Tianjin Municipal Natural Science Foundation of China (14JCZDJC32200 and 13JCZDJC33900), Open Project of Key Laboratory of Functional Inorganic Material Chemistry (Heilongjiang University), Ministry of Education of China, Academic Innovation Funding of Tianjin Normal University (52XC1404), LPMT, CAEP (KF14006), Training Plan of Leader Talent of University in Tianjin, Scientific Research Foundation for Returned Overseas Chinese Scholars of State Education Ministry, and the program of Thousand Youth Talents in Tianjin of China.

Appendix A. Supplementary data

Supplementary data associated with this article can be found, in the online version, at <http://dx.doi.org/10.1016/j.electacta.2015.06.041>.

References

- [1] A.L. Mohana Reddy, S.R. Gowda, M.M. Shaijumon, P.M. Ajayan, Hybrid nanostructures for energy storage applications, *Adv. Mater.* 24 (2012) 5045–5064.
- [2] X. Li, C. Wang, Engineering nanostructured anodes via electrostatic spray deposition for high performance lithium ion battery application, *J. Mater. Chem. A* 1 (2013) 165–182.
- [3] S. Pei, J. Zhao, J. Du, W. Ren, H.-M. Cheng, Direct reduction of graphene oxide films into highly conductive and flexible graphene films by hydrohalic acids, *Carbon* 48 (2010) 4466–4474.
- [4] V. Georgakilas, M. Otyepka, A.B. Bourlinos, V. Chandra, N. Kim, K.C. Kemp, P. Hobza, R. Zboril, K.S. Kim, Functionalization of graphene: covalent and non-covalent approaches, derivatives and applications, *Chem. Rev.* 112 (2012) 6156–6214.
- [5] M. Hu, X. Pang, Z. Zhou, Recent progress in high-voltage lithium ion batteries, *J. Power Sources* 237 (2013) 229–242.
- [6] L. Jiang, Z. Fan, Design of advanced porous graphene materials: from graphene nanomesh to 3D architectures, *Nanoscale* 6 (2014) 1922–1945.
- [7] A. Chavez-Valdez, M.S. Shaffer, A.R. Boccaccini, Applications of graphene electrophoretic deposition. A review, *J. Phys. Chem. B* 117 (2013) 1502–1515.
- [8] S. Yang, X. Feng, L. Wang, K. Tang, J. Maier, K. Mullen, Graphene-based nanosheets with a sandwich structure, *Angew. Chem. Int. Ed. Engl.* 49 (2010) 4795–4799.
- [9] J.-Y. Lin, G. Yue, S.-Y. Tai, Y. Xiao, H.-M. Cheng, F.-M. Wang, J. Wu, Hydrothermal synthesis of graphene flake embedded nanosheet-like molybdenum sulfide hybrids as counter electrode catalysts for dye-sensitized solar cells, *Mater. Chem. Phys.* 143 (2013) 53–59.
- [10] I.Y.Y. Bu, Highly conductive and transparent reduced graphene oxide/aluminum doped zinc oxide nanocomposite for the next generation solar cell applications, *Opt. Mater.* 36 (2013) 299–303.
- [11] A. Hu, X. Chen, Q. Tang, Z. Liu, B. Zeng, One-step synthesis of Fe₃O₄@C/reduced-graphene oxide nanocomposites for high-performance lithium ion batteries, *J. Phys. Chem. Solids* 75 (2014) 588–593.
- [12] C. Wang, D. Li, C.O. Too, G.G. Wallace, Electrochemical Properties of Graphene Paper Electrodes Used in Lithium Batteries, *Chem. Mater.* 21 (2009) 2604–2606.
- [13] S. Yang, X. Feng, S. Ivanovici, K. Mullen, Fabrication of graphene-encapsulated oxide nanoparticles: towards high-performance anode materials for lithium storage, *Angew. Chem. Int. Ed. Engl.* 49 (2010) 8408–8411.
- [14] Y. Bai, R.B. Rakhi, W. Chen, H.N. Alshareef, Effect of pH-induced chemical modification of hydrothermally reduced graphene oxide on supercapacitor performance, *J. Power Sources* 233 (2013) 313–319.
- [15] X. Wang, T. Wang, C. Yang, H. Li, P. Liu, Well-defined flake-like polypyrrole grafted graphene nanosheets composites as electrode materials for supercapacitors with enhanced cycling stability, *Appl. Surf. Sci.* 287 (2013) 242–251.
- [16] D. Cai, S. Wang, L. Ding, P. Lian, S. Zhang, F. Peng, H. Wang, Superior cycle stability of graphene nanosheets prepared by freeze-drying process as anodes for lithium-ion batteries, *J. Power Sources* 254 (2014) 198–203.
- [17] X. Li, D. Geng, Y. Zhang, X. Meng, R. Li, X. Sun, Superior cycle stability of nitrogen-doped graphene nanosheets as anodes for lithium ion batteries, *Electrochem. Commun.* 13 (2011) 822–825.
- [18] L.L. Tian, X.Y. Wei, Q.C. Zhuang, C.H. Jiang, C. Wu, G.Y. Ma, X. Zhao, Z.M. Zong, S. G. Sun, Bottom-up synthesis of nitrogen-doped graphene sheets for ultrafast lithium storage, *Nanoscale* 6 (2014) 6075–6083.
- [19] X. Li, Y. Hu, J. Liu, A. Lushington, R. Li, X. Sun, Structurally tailored graphene nanosheets as lithium ion battery anodes: an insight to yield exceptionally high lithium storage performance, *Nanoscale* 5 (2013) 12607–12615.

- [20] J. Liu, Y. Wan, W. Liu, Z. Ma, S. Ji, J. Wang, Y. Zhou, P. Hodgson, Y. Li, Mild and cost-effective synthesis of iron fluoride-graphene nanocomposites for high-rate Li-ion battery cathodes, *J. Mater. Chem. A* 1 (2013) 1969.
- [21] Q. Fan, L. Lei, X. Xu, G. Yin, Y. Sun, Direct growth of FePO₄/graphene and LiFePO₄/graphene hybrids for high rate Li-ion batteries, *J. Power Sources* 257 (2014) 65–69.
- [22] X. Li, X. Meng, J. Liu, D. Geng, Y. Zhang, M.N. Banis, Y. Li, J. Yang, R. Li, X. Sun, M. Cai, M.W. Verbrugge, Tin Oxide with Controlled Morphology and Crystallinity by Atomic Layer Deposition onto Graphene Nanosheets for Enhanced Lithium Storage, *Adv. Funct. Mater.* 22 (2012) 1647–1654.
- [23] Z.-S. Wu, G. Zhou, L.-C. Yin, W. Ren, F. Li, H.-M. Cheng, Graphene/metal oxide composite electrode materials for energy storage, *Nano Energy* 1 (2012) 107–131.
- [24] S.H. Ha, Y.S. Jeong, Y.J. Lee, Free Standing Reduced Graphene Oxide Film Cathodes for Lithium Ion Batteries, *ACS Appl. Mater. Interfaces* 5 (2013) 12295–12303.
- [25] B.Z. Jang, C. Liu, D. Neff, Z. Yu, M.C. Wang, W. Xiong, A. Zhamu, Graphene surface-enabled lithium ion-exchanging cells: next-generation high-power energy storage devices, *Nano Lett.* 11 (2011) 3785–3791.
- [26] H. Kim, H.D. Lim, S.W. Kim, J. Hong, D.H. Seo, D.C. Kim, S. Jeon, S. Park, K. Kang, Scalable functionalized graphene nano-platelets as tunable cathodes for high-performance lithium rechargeable batteries, *Sci. Rep.* 3 (2013) 1506.
- [27] W. Ai, Z. Du, Z. Fan, J. Jiang, Y. Wang, H. Zhang, L. Xie, W. Huang, T. Yu, Chemically engineered graphene oxide as high performance cathode materials for Li-ion batteries, *Carbon* 76 (2014) 148–154.
- [28] Z.-j. Jiang, Z. Jiang, W. Chen, The role of holes in improving the performance of nitrogen-doped holey graphene as an active electrode material for supercapacitor and oxygen reduction reaction, *J. Power Sources* 251 (2014) 55–65.
- [29] C.T. Chien, S.S. Li, W.J. Lai, Y.C. Yeh, H.A. Chen, I.S. Chen, L.C. Chen, K.H. Chen, T. Nemoto, S. Isoda, M. Chen, T. Fujita, G. Eda, H. Yamaguchi, M. Chhowalla, C.W. Chen, Tunable photoluminescence from graphene oxide, *Angew. Chem. Int. Ed. Engl.* 51 (2012) 6662–6666.
- [30] T. Sakthivel, V. Gunasekaran, S.J. Kim, Effect of oxygenated functional groups on the photoluminescence properties of graphene-oxide nanosheets, *Mater. Sci. Semicond. Process* 19 (2014) 174–178.
- [31] K. Krishnamoorthy, U. Navaneethaiyer, R. Mohan, J. Lee, S.-J. Kim, Graphene oxide nanostructures modified multifunctional cotton fabrics, *Appl. Nanosci.* 2 (2011) 119–126.
- [32] G. Venugopal, K. Krishnamoorthy, R. Mohan, S.-J. Kim, An investigation of the electrical transport properties of graphene-oxide thin films, *Mater. Chem. Phys.* 132 (2012) 29–33.
- [33] K. Krishnamoorthy, M. Veerapandian, K. Yun, S.J. Kim, The chemical and structural analysis of graphene oxide with different degrees of oxidation, *Carbon* 53 (2013) 38–49.
- [34] K. Kakaei, k. hasanpour, Synthesis of graphene oxide nanosheets by electrochemical exfoliation of graphite in cetyltrimethylammonium bromide and its application for oxygen reduction, *J. Mater. Chem. A* 2 (2014) 15428–15436.
- [35] X. Han, C. Chang, L. Yuan, T. Sun, J. Sun, Aromatic Carbonyl Derivative Polymers as High-Performance Li-Ion Storage Materials, *Adv. Mater.* 19 (2007) 1616–1621.
- [36] T. Gall, K. Reiman, M. Gressel, J. Owen, Poly(2, 5-dihydroxy-1, 4-benzoquinon-3, 6-methylene): a new organic polymer as positive electrode material for rechargeable lithium batteries, *J. Power Sources* 119 (2003) 316–320.
- [37] H. Buqa, D. Goers, M. Holzapfel, M.E. Spahr, P. Novak, High Rate Capability of Graphite Negative Electrodes for Lithium-Ion Batteries, *J. Electrochem. Soc.* 152 (2005) A474.
- [38] Z. Song, T. Xu, M.L. Gordin, Y.-B. Jiang, I.-T. Bae, Q. Xiao, H. Zhan, J. Liu, D. Wang, Polymer-Graphene Nanocomposites as Ultrafast-Charge and -Discharge Cathodes for Rechargeable Lithium Batteries, *Nano Lett.* 12 (2012) 2205–2211.
- [39] D. Wang, J. Yang, X. Li, D. Geng, R. Li, M. Cai, T.-K. Sham, X. Sun, Layer by layer assembly of sandwiched graphene/SnO₂ nanorod/carbon nanostructures with ultrahigh lithium ion storage properties, *Energy Environ. Sci.* 6 (2013) 2900.
- [40] B. Luo, L. Zhi, Design and construction of three dimensional graphene-based composites for lithium ion battery applications, *Energy Environ. Sci.* 8 (2014) 456–477.
- [41] N. Nitta, F. Wu, J.T. Lee, G. Yushin, Li-ion battery materials: present and future, *Mater. Today* 18 (2014) 252–264.
- [42] H. Buqa, D. Goers, M. Holzapfel, M.E. Spahr, P. Novak, High Rate Capability of Graphite Negative Electrodes for Lithium-Ion Batteries, *J. Electrochem. Soc.* 152 (2005) A474.
- [43] X. Yu, C. Zhan, R. Lv, Y. Bai, Y. Lin, Z.-H. Huang, W. Shen, X. Qiu, F. Kang, Ultrahigh-rate and high-density lithium-ion capacitors through hybridizing nitrogen-enriched hierarchical porous carbon cathode with prelithiated microcrystalline graphite anode, *Nano Energy* 15 (2015) 43–53.
- [44] K. Zhang, H. Wang, X. He, Z. Liu, L. Wang, L. Gu, H. Xu, P. Han, S. Dong, C. Zhang, J. Yao, G. Cui, L. Chen, A hybrid material of vanadium nitride and nitrogen-doped graphene for lithium storage, *J. Mater. Chem.* 21 (2011) 11916.